Developing EGFR-Targeted Nanoliposomal Therapeutics in Head and Neck Squamous Cell Carcinoma

A Technical Report

in STS4600

Presented to

The Faculty of the

School of Engineering and Applied Science

University of Virginia

In Partial Fulfillment of the Requirements for the Degree

Bachelor of Science in Biomedical Engineering

Patrick James Beck

May 4, 2020

Technical Project Team Members:
Sally Greenberg
Abhishek Karkar
An Smith

Approved by Prof. Mark Kester, Department of Pharmacology

Abstract

Head and Neck Squamous Cell Carcinoma (HNSCC) is the 7th most common cancer worldwide. Despite its prevalence, Cetuximab is the only HNSCC-targeted therapy that exists to treat it, which has shown mixed outcomes in patients. This highlights the need to develop more effective treatment options for HNSCC patients. The ceramide nanoliposome (CNL) is a cancer cell death-inducing therapeutic currently in Phase I clinical trials for multiple cancers. The Kester Lab at the University of Virginia has identified a synergistic cell death effect between CNL and Erlotinib or Gefitinib, two FDA-approved drugs with the same molecular target as Cetuximab. The purpose of this study was to fully investigate the combination of CNL and Erlotinib, Gefitinib, or Cetuximab and prepare these combinations for use in living-organism HNSCC trials. Through successive cell viability experiments, synergy was confirmed between CNL and Erlotinib or Gefitinib, while no synergy was found between CNL and Cetuximab. To improve bloodstream retention time and host immune system shielding, Erlotinib and Gefitinib were successfully encapsulated inside their own lipid nanoparticle delivery vehicles. Optimization of the delivery vehicle compositions to deliver a maximal drug payload was in progress until this study was interrupted by the Covid-19 pandemic. Cetuximab was attempted to be attached to the CNL particle surface to serve as a molecular targeting mechanism, but success was never reached due to the institution of remote learning. This study characterized a novel combinatorial effect between CNL and Erlotinib or Gefitinib and laid the groundwork for future targeted delivery systems to combat HNSCC.

Introduction

Head and Neck Squamous Cell Carcinoma (HNSCC) is the seventh most common form of cancer worldwide with approximately 875,000 new HNSCC cases diagnosed each year (Bray et al., 2018). HNSCC develops in squamous cells of the mucous membranes of the mouth, nose, and throat, specifically arising from regions such as the lip, oral cavity, pharynx, and larynx (Mao et al., 2004). Although recent advancements in cancer diagnostics and treatments have been made, many patients are diagnosed at advanced stages and cannot be treated using conventional treatment methods such as surgery, chemotherapy, and radiotherapy (Byeon et al., 2019). Alternate treatment methods have focused on targeted drug therapy, specifically targeting the Epidermal Growth Factor Receptor (EGFR). EGFR is overexpressed in 40-80% of HNSCC (Sheu et al., 2009) and elevated protein levels have been found to correlate with worse disease prognosis (Grandis et al., 1998).

Recently, two immune checkpoint inhibitors were approved for use in HNSCC, but they have been found to only deliver modest benefits to patients (Sim et al., 2019). Prior to 2019, a monoclonal antibody, Cetuximab (Erbitux®), was the only FDA-approved pharmacological treatment for HNSCC patients. Cetuximab is a targeted inhibitor of EGFR, binding the EGFR extracellular ligand-binding domain with higher affinity than natural ligands and blocking downstream pathway signaling (Mehra et al., 2008). Cetuximab alone has shown limited success in treating HNSCC, only extending patient survival on the scale of months (Vermorken et al., 2008), while demonstrating a risk for allergic reaction in a subset of patients (O'Neil et al., 2007). Additionally, the development of drug resistance has been common (Chen et al., 2010; Vermorken et al., 2007). The apparent shortcomings of Cetuximab underscore the need to develop more effective HNSCC treatment methods.

The ceramide nanoliposome (CNL) is a nanoscale therapeutic that recently passed Phase I clinical trials. CNL consists of the signaling sphingolipid C_6-ceramide, which has been previously implicated in the induction of cell cycle arrest and apoptosis (Kolesnick and Krönke, 1998; Merrill et al., 1997), encapsulated inside a lipid nanoparticle. CNL has shown efficacy in multiple *in vitro* and *in vivo* cancer models (Dhule et al., 2014; Stover and Kester, 2003; Stover et al., 2005; Watters et al., 2012), while also demonstrating the ability to combine successfully with other chemotherapeutics and enhance their effectiveness (Adiseshaiah et al., 2013; Jiang et al., 2011; Tran et al., 2008). Recent unpublished data generated from the Kester Lab at the University of Virginia has provided evidence that CNL sensitizes HNSCC cell lines to Erlotinib and Gefitinib, two EGFR tyrosine kinase domain inhibitors that had both previously failed to show significant clinical benefit as single agents in HNSCC clinical trials (Perez et

al., 2012; Soulieres et al., 2004). The emergence of this effect provides a rationale that CNL may induce the same effect in HNSCC cells treated with Cetuximab. Even moreso, given the properties of Cetuximab as a chimeric monoclonal antibody, the potential to use Cetuximab as a CNL-surface targeting motif exists irrespective of a combinatorial effect.

The purpose of this study will be to fully explore the potential of a combinatorial therapy between CNL and Erlotinib, Gefitinib, or Cetuximab. Each of the three combinations will be examined for efficacy in HNSCC *in vitro* models. If efficacy is observed, steps will be taken to prepare these combinatorial therapies for *in vivo* testing. Specifically, Erlotinib and Gefitinib will be encapsulated inside individual liposomes, and successful conjugation of Cetuximab to the surface of the CNL will be attempted. This study hopes to make significant progress toward developing more effective and targeted drug therapies for patients with HNSCC.

Results

EGFR Inhibitors and CNL as Single Agents in HNSCC

This study first aimed to fully explore the efficacy of each of the three EGFR inhibitors, Erlotinib, Gefitinib, and Cetuximab, and CNL in HNSCC as single agents. To accomplish this, two HNSCC cell lines, UNC-7 and SCC-25, were treated with varying concentrations of each of the EGFR inhibitors and CNL and cell viability was measured at 24- and 48-hours post-treatment. The concentration ranges for each drug were determined based on physiologically relevant concentrations identified by prior studies literature.

Erlotinib and Gefitinib failed to reduce cell viability by more than 31% in either cell line at the 24-hour time point (Erlotinib/Gefitinib, Figure 1A). At 48 hours post-treatment, Erlotinib failed to show anything beyond marginal decreases in cell viability (Erlotinib, Figure 1B). Gefitinib did show a slight time-dependent effect at the 48-hour time point, with the UNC-7 cell line demonstrating a 44% decrease in cell viability at the highest concentration; however, non-maximum Gefitinib concentrations remained nearly 100% viable (Gefitinib, Figure 1B). From these data, Erlotinib and Gefitinib are confirmed to be minimally effective as monotherapies for HNSCC.

Cetuximab failed to show any sort of efficacy in the UNC-7 cell line at either time point (Cetuximab, Figure 1). Data was not available for the SCC-25 cell line at either time point due to cell line contamination and virtual education constraints.

In contrast with all three EGFR inhibitors, CNL did show significant efficacy as a single agent in HNSCC. At the 24-hour time point, CNL demonstrated a strong concentration-dependent effect in both cell lines, decreasing cell viability at the highest concentration to 45% and 43% in the UNC-7 and SCC-25 cell lines, respectively (CNL, Figure 1A). The efficacy of CNL increased at 48 hours post-treatment, evidencing an additional time-dependent effect, with UNC-7 cells dropping to 27% viability at the highest concentration and SCC-25 cells dropping further to 15% viability (CNL, Figure 1B). These results reveal the strong therapeutic potential of CNL as a single agent in HNSCC.

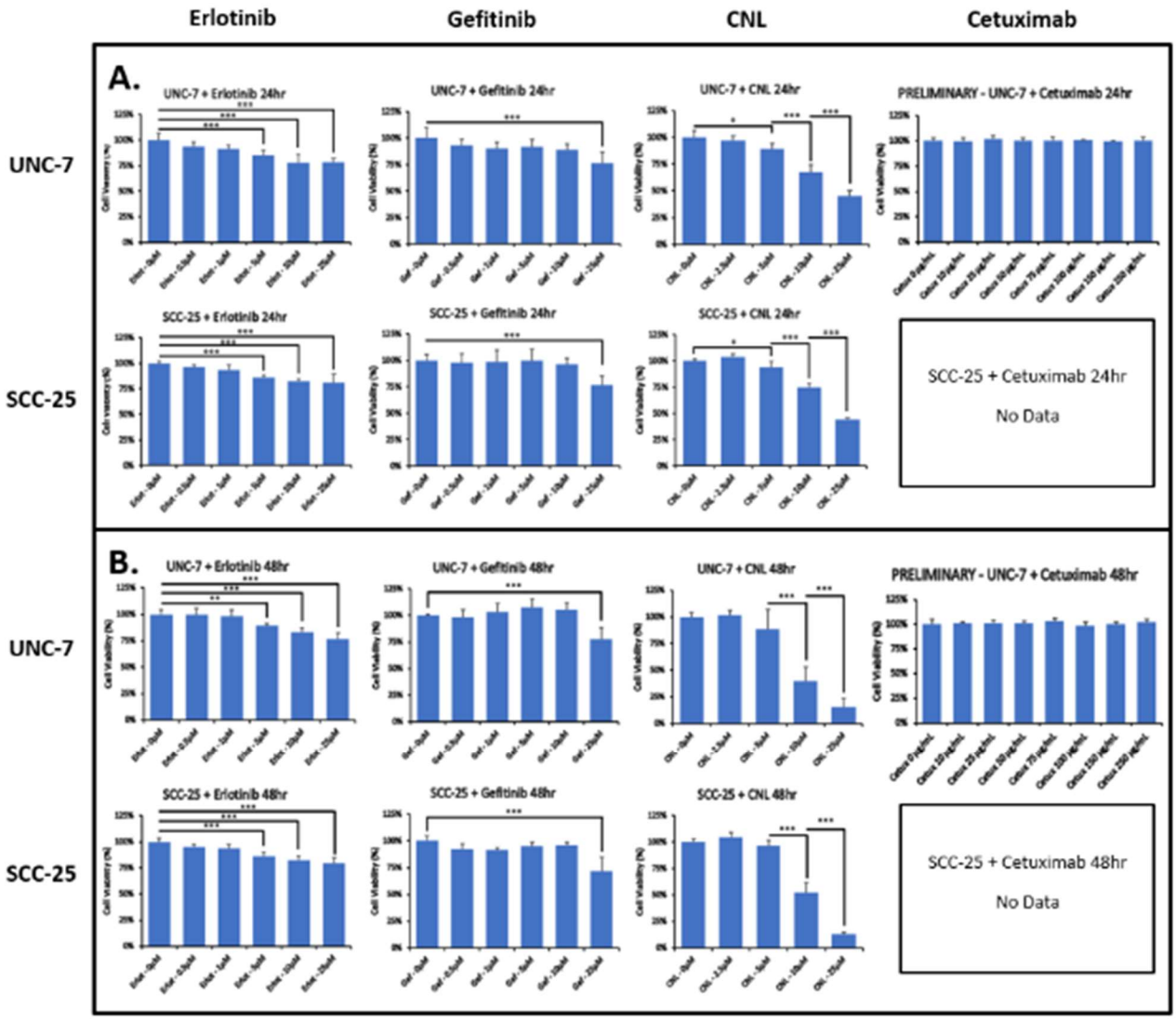

Figure 1. Cell viability of two HNSCC cell lines treated with varying concentrations of four different pharmacological agents at two time points. Panel A shows cell viability at 24 hours post-treatment and Panel B shows cell viability at 48 hours post-treatment. Within each panel, the top row shows the response of UNC-7 cells subjected to each treatment while the bottom row shows the response of SCC-25 cells. From left to right, the columns show the response of cells treated with Erlotinib, Gefitinib, CNL, and Cetuximab. For all Erlotinib, Gefitinib, and CNL plots, a total of three biological replicates were collected. For the UNC-7 Cetuximab plots, one biological replicate was collected. No data was available for SCC-25 cells treated with Cetuximab. Within each plot, all concentrations were normalized to the value of the zero drug condition. '***' indicates p-value < 0.001, '**' indicates p-value < 0.01, and '*' indicates p-value < 0.05.

Combination of CNL + EGFR Inhibitors in HNSCC

Given the lack of response to each of the EGFR inhibitors alone, this study investigated if combination with CNL could sensitize HNSCC cells to Erlotinib, Gefitinib, and Cetuximab. The same two HNSCC cell lines were first pre-treated with varying concentrations either Erlotinib, Geftinib, or Cetuximab for one hour after which varying concentrations of CNL were added. Cell viability was measured at 24 and 48 hours post-CNL treatment. In the event that synergy or antagonism between the combined drugs was identified, Bliss synergy scores were calculated to determine the magnitude of the effect.

CNL was able to synergistically sensitize both UNC-7 and SCC-25 cells to Erlotinib. At the 24-hour time point (Erlotinib+CNL, Figure 2A), little to no synergy is observed between CNL and Erlotinib in either cell line. Any changes in cell viability are calculated to be solely a function of the additive effects between both drugs individually. Measuring cell viability at 48 hours post-treatment, synergy can be identified in both cell lines (Erlotinib+CNL, Figure 2B). Erlotinib at 10 or 25μM combined with CNL at 5 or 10μM seem to deliver the most potent synergy (Erlotinib+CNL, Figure 2B). Specifically, in the SCC-25 cell line at the 48-hour time point, cells treated separately with 5μM CNL or 25μM Erlotinib were 95% and 83% viable, respectively (Erlotinib+CNL, Figure 2B). Addition would predict the combination to yield cells that are 78% viable, but in actuality, they are 49% viable (Erlotinib+CNL, Figure 2B). Bliss synergy scores at the 48-hour time point were calculated to be 10.48 and 6.05 for the UNC-7 and SCC-25 cell lines, respectively. As positive Bliss scores are indicative of synergy, this analysis mathematically confirmed synergy between Erlotinib and CNL.

An even stronger synergistic effect was observed between Gefitinib and CNL. Synergy between Gefitinib and CNL was identified as early as 24 hours post-treatment (Gefitinib+CNL, Figure 2A). Specifically, the Bliss scores for the UNC-7 and SCC-25 cell lines at the 24-hour time point were 10.68 and 7.22, respectively. Similar to the combination of Erlotinib and CNL, the points of synergy are primarily at high concentrations of Gefitinib and middle concentrations of CNL. Specifically, both cell lines demonstrate strong synergy at intersections between 10 or 25μM Gefitinib combined with 5 or 10μM CNL. Some of the most striking instances of synergy can be observed at the 48-hour time point (Gefitinib+CNL, Figure 2B). Specifically, in the SCC-25 cell line, cells treated separately with 5μM CNL or 10μM Gefitinib were 96% and 102% viable, respectively (Gefitinib+CNL, Figure 2B). The additive effect would predict cells treated with the combination to be 98% viable, but instead, cells that are 35% viable are observed (Gefitinib+CNL, Figure 2B). Bliss scores were calculated to be 18.50 for the UNC-7 cell line and 16.10 for the SCC-25 cell line at the 48-hour time point, again confirming strong synergy between Gefitinib and CNL. The identification of a synergistic effect between CNL and both Erlotinib and Gefitinib provides a strong rationale of therapeutic efficacy for these drug combinations.

In contrast with Erlotinib and Gefitinib, CNL failed to induce synergistic cell death when combined with Cetuximab. Notably, CNL was able to sensitize UNC-7 cells to Cetuximab at both time points, but no additional synergy was observed beyond the additive effects of CNL and Cetuximab as single agents (Cetuximab+CNL, Figure 1). Data was not available for the SCC-25 cell line at either time point due to cell line contamination and virtual education constraints.

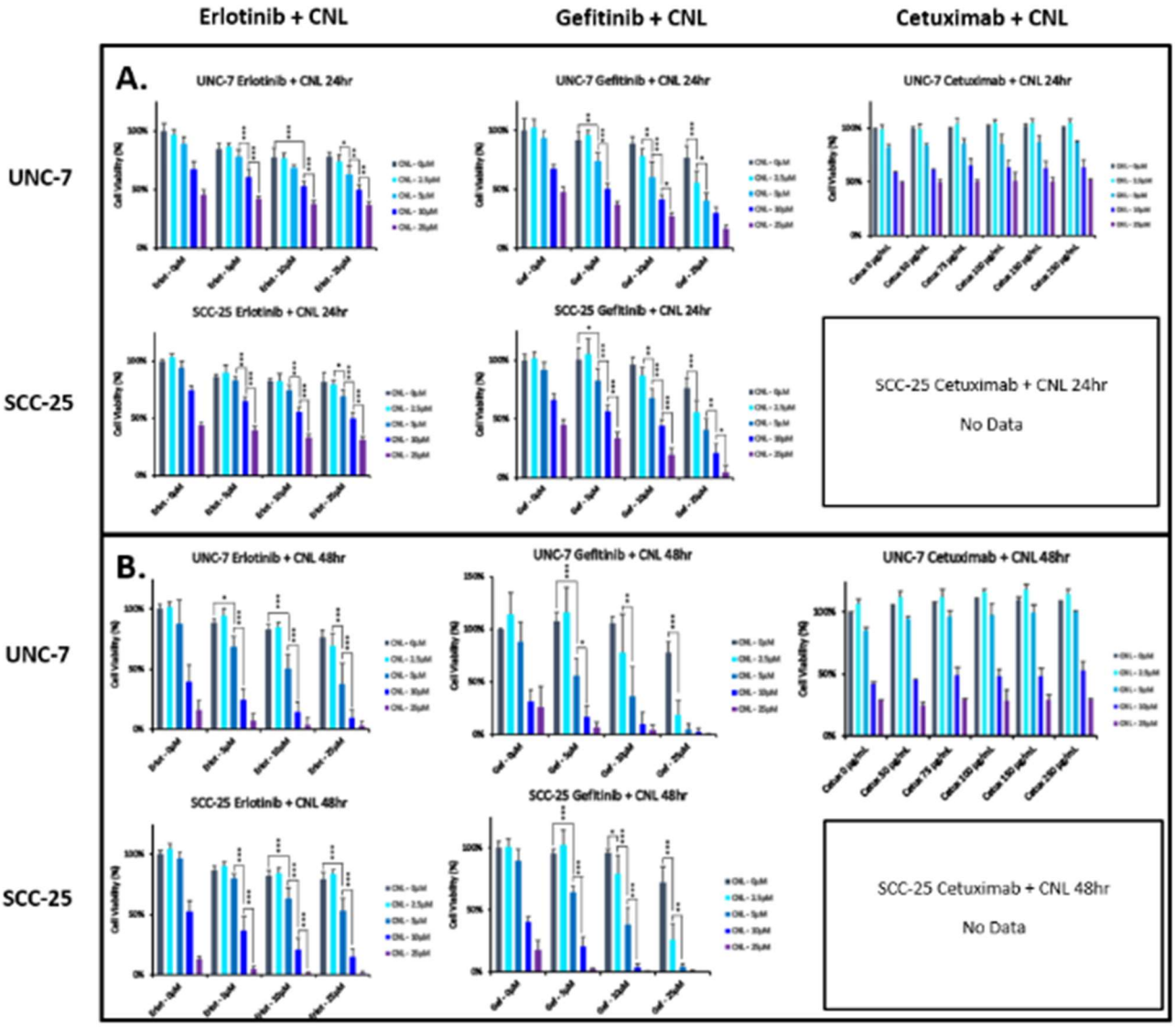

Figure 2. Cell viability of two HNSCC cell lines treated with varying concentrations of CNL combined with varying concentrations of three different pharmacological agents at two time points. Specifically, five concentrations of CNL were combined with six concentrations of Erlotinib, Gefitinib, or Cetuximab. Cells were pre-treated with Erlotinib, Gefitinib, or Cetuximab for one hour prior to CNL treatment. Panel A shows cell viability at 24 hours post-CNL treatment and Panel B shows cell viability at 48 hours post-CNL treatment. Within each panel, the top row shows the response of UNC-7 cells subjected to each treatment while the bottom row shows the response of SCC-25 cells. From left to right, the columns show the response of cells treated with the combination of Erlotinib + CNL, Gefitinib + CNL, and Cetuximab + CNL. For all Erlotinib + CNL and Gefitinib + CNL plots, a total of three biological replicates were collected. For the UNC-7 Cetuximab + CNL plots, one biological replicate was collected. No data was available for SCC-25 cells treated with Cetuximab and CNL. Within each plot, all concentrations were normalized to the value of the double zero drug condition. For Erlotinib + CNL and Gefitinib + CNL, the two lower concentrations of each inhibitor were ignored because no synergy was observed at these concentrations in any cell line at either time point. '***' indicates p-value < 0.001, '**' indicates p-value < 0.01, and '*' indicates p-value < 0.05.

Liposomal Encapsulation of Erlotinib and Gefitinib

Under the guidance of the Kester Lab at the University of Virginia, the components of the EGFR inhibitor liposomes were decided to be each drug itself combined with 1,2-distearoyl-sn-glycero-3-phosphocholine (DSPC), 1,2-dioleoyl-sn-glycero-3-phosphoethanolamine (DOPE), and 1,2-distearoyl-sn-glycero-3-phosphoethanolamine-N-[amino(polyethylene glycol)-2000] (DSPE-PEG(2000)). DSPC and DOPE were set to serve as the base components of the liposomal membrane, while the inclusion of PEGylated phospholipids conferred the functions of increased bloodstream retention time and immune system shielding. The above components were combined according to the molar ratios in Figure 3 and the thin-film hydration method followed by extrusion with a 100 nm Nuclepore filter were used to form liposomes approximately 90-100 nm in size. Following extrusion, liposome size and zeta potential were measured by Dynamic Light Scattering (DLS). Size-exclusion column chromatography was used to separate the liposomes from the non-encapsulated drug in the surrounding solution before liposomal aliquots were given to Dr. Todd Fox in the Kester Lab for encapsulation efficiency measurement by mass spectrometry. Figure 3 shows the results for the first successful batch of Erlotinib- and Gefitinib-encapsulated liposomes

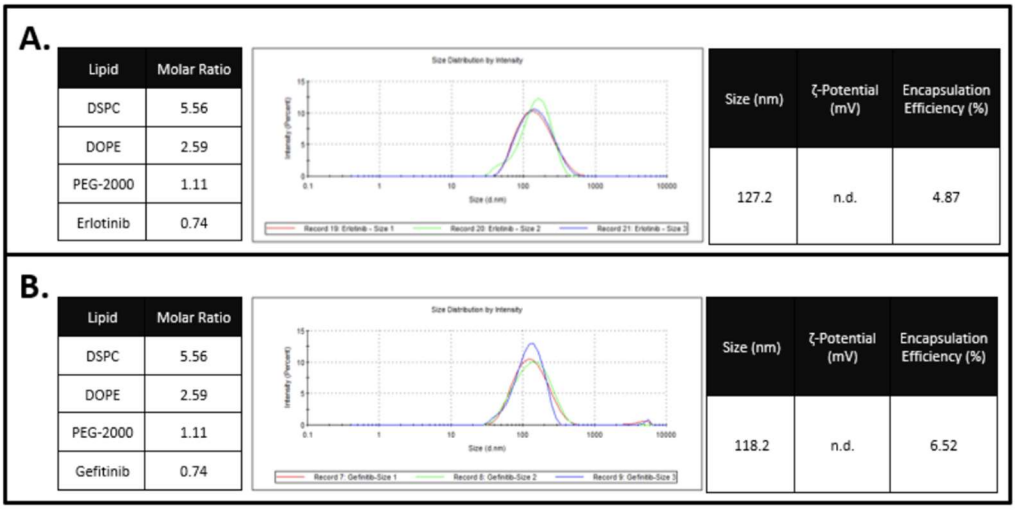

Figure 3. Lipid composition, size, and encapsulation efficiency for the first attempt at encapsulating Erlotinib and Gefitinib inside liposomes. DLS was used to measure the size distribution of Erlotinib-encapsulated liposomes (Panel A) and Gefitinib-encapsulated liposomes (Panel B). Within each panel, the left table displays the relative quantities of each lipid component in the formulation as a molar ratio. The center figure shows the size distribution by intensity of the produced batch of liposomes. Three measurements were collected during the sizing of each liposome batch. The right table displays the average size of the liposomes in the batch and its encapsulation efficiency. Encapsulation efficiency was measured using mass spectrometry. ζ-potential was not measured due to technical equipment difficulties.

The diameters for the Erlotinib- and Gefitinib-encapsulated liposomes were measured to be 127.2 nm ± 0.8 nm and 118.2 ± 1.2 nm, respectively (Figure 3). These sizes are notably larger than the pore size of the 100 nm filter. During extrusion, the filter had to be changed to a 200 nm pore size due to the difficulty and repeated rupturing of the smaller-sized filter. This challenge likely indicated a degree of improper liposome formation. Despite this difficulty, the size distributions of the liposomes were still measured to be appropriately narrow and bell-shaped (Figure 3). Due to the combination of user error and virtual education constraints, zeta potential data were not available. The encapsulation efficiencies were well below the target of 25-30% that was established for this study (Figure 3). To address this shortcoming, a second batch of each of the liposomes was planned.

Alterations were made to each liposome composition in an effort to increase the encapsulation efficiencies. This study hypothesized that a reason for the low encapsulation efficiencies could be that in the time between extrusion and column chromatography, a quantity of each drug leaked out of the liposome into the surrounding solution. As such, cholesterol was added to each formulation in place of DOPE to prohibit this leaking effect (Kirby et al., 1980). Using feedback from the Kester Lab, the liposome molar ratios were altered slightly, most notably decreasing the amount of each drug added to ensure adequate lipids were available for liposome formation (Figure 4). In addition, two key changes were introduced to the thin-film hydration protocol. Following the combination of each of the liposome components, the lipid drying time was increased to ensure all chloroform had evaporated prior to rehydration, while in between the sonication and extrusion steps, the liposomes were left shaking at 60˚C instead of being allowed to begin to cool and solidify near room temperature. With all of these alterations introduced, a second batch of liposomes was successfully produced

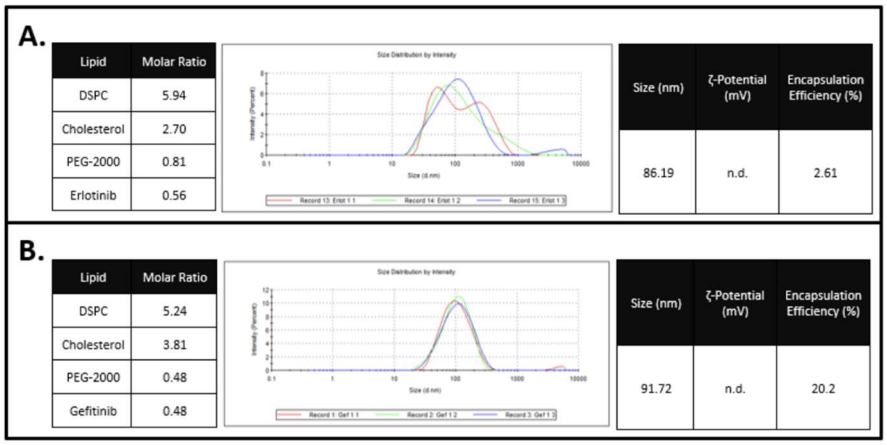

Figure 4. Lipid composition, size, and encapsulation efficiency for the second attempt at encapsulating Erlotinib and Gefitinib inside liposomes. DLS was used to measure the size distribution of Erlotinib-encapsulated liposomes (Panel A) and Gefitinib-encapsulated liposomes (Panel B). Within each panel, the left table displays the relative quantities of each lipid component in the formulation as a molar ratio. Relative to the first attempt, the lipid composition and molar ratios were changed slightly in an effort to improve the encapsulation efficiencies. The center figure shows the size distribution by intensity of the produced batch of liposomes. Three measurements were collected during the sizing of each liposome batch. The right table displays the average size of the liposomes in the batch and its encapsulation efficiency. Encapsulation efficiency was measured using mass spectrometry. ζ-potential was not measured due to technical equipment difficulties.

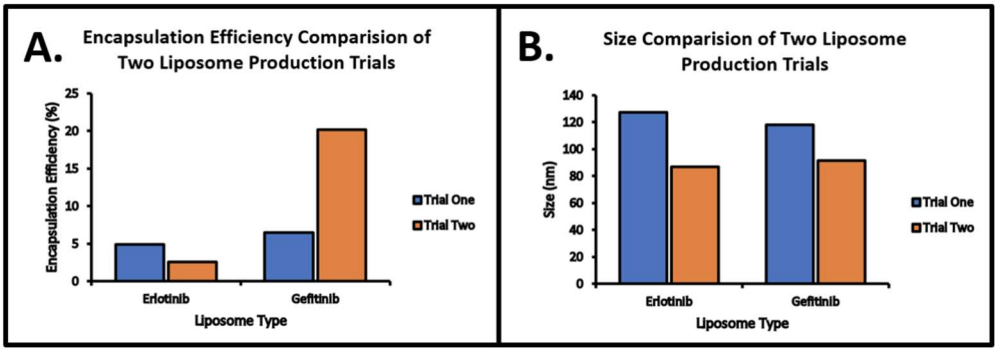

Figure 5. A comparison of liposome encapsulation efficiency (Panel A) and size (Panel B) for two trials of producing both Erlotinib- and Gefitinib-encapsulated liposomes. Liposome sizing improved between the first and second attempt as the measured sizing approached the target range of 90-100 nm. Between the first and second attempt, encapsulation efficiency improved for Gefitinib, while a slight decline was observed in Erlotinib encapsulation.

The diameters for the Erlotinib- and Gefitinib-encapsulated liposomes for the second batch were measured to be 86.2 nm ± 0.9 nm and 91.7 nm ± 0.3 nm, respectively (Figure 4). Figure 5 offers a comparison between the first and second batches of each liposome. The second batch of liposomes are markedly smaller in diameter than the first batch (Figure 5B). During extrusion, the second batch of liposomes passed smoothly through the 100 nm filter, indicating that the changes introduced were likely beneficial. The size distribution of the Gefitinib liposomes were consistent and appropriately narrow (Figure 4B). The size distribution of the Erlotinib liposomes was notably larger and less consistency existed between measurement replications (Figure 4A). Due to the combination of user error and virtual education constraints, zeta potential data were again not available. Strikingly, the alterations to the Gefitinib liposome formulation increased the encapsulation efficiency to 20.2% (Figure 4B). This was an increase in encapsulation efficiency of nearly 14% compared to the first batch (Figure 5A). In contrast, the encapsulation efficiency of the Erlotinib liposomes decreased slightly to 2.61% (Figure 4A). A third batch of Erlotinib liposomes was being planned to directly address this persistently low encapsulation efficiency, but was interrupted by the transition to virtual education.

Stability and Efficacy of Encapsulated Erlotinib and Gefitinib

This section was part of this study's original specific aims. However, due to the interruption by the transition to virtual education, it was not completed. The study's planned protocol and anticipated results will still be addressed.

Following optimizing the formulations of each of the EGFR inhibitor liposomes, the "long-term" stability of both of the liposomes would be measured over the course of one month. Specifically, aliquots of both the Erlotinib- and Gefitinib-encapsulated liposomes would be subjected to a range of BSA protein concentrations, pH's, and temperatures to simulate *in vivo* conditions. The size and zeta potential of the samples subjected to each of the conditions would be measured weekly by DLS to track changes in liposome stability. Figure 6 displays the study's predicted results for these experiments.

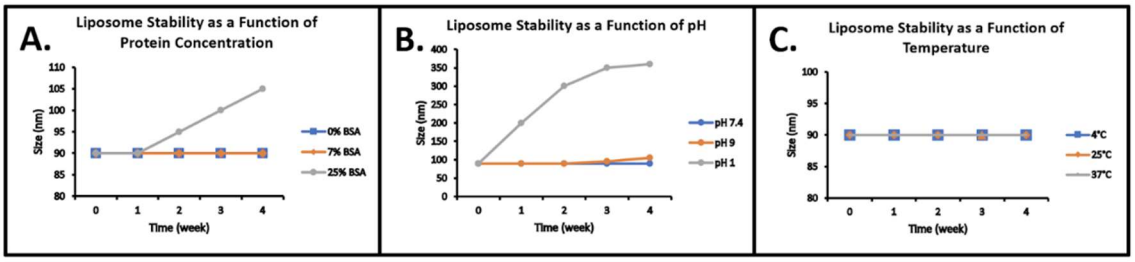

Figure 6. Our predicted results for liposome stability as a function of BSA protein concentration (Panel A), pH (Panel B), and temperature (Panel C) over time. Liposome pH would have been varied using a buffer solution to physiologically-relevant pHs of 1, 7.4, and 9. Liposome formulations would have been stored at temperatures of 4°C (refrigerator), 25° (room temperature), and 37°C (body temperature). Protein concentration in the solution surrounding the liposomes would have been varied to physiologically-relevant values of 0%, 7%, and 25% BSA. Size distributions would have been measured using DLS each week over a period of four weeks. Three measurements would have been collected during the sizing of the liposome batch. Our predicted average sizes are shown against each time point for each condition.

The study predicted that at 0% and 7% BSA, liposome stability would not be affected (Figure 6A). However, as BSA concentration increased to 25%, it was predicted that increasing charge interactions between the positively-charged PEG on the liposome surface and negatively-charged residues or regions of the BSA protein would begin to create liposome-protein aggregates, leading to greater measured sizes (Figure 6A). With respect to pH stability, the study predicted that the liposomes would be

stable at pH 7.4, as they are routinely stored in pH 7.4 Phosphate Buffered Saline (PBS) (Figure 6B). Liposomes were predicted to be relatively stable at pH 9, given its proximity to pH 7.4, but it was predicted that exposing the liposomes to pH 1 for a four-week period would ultimately dissolve the liposomes in the strong acidic environment (Figure 6B). Finally, liposomes were predicted to be stable across all selected temperatures, as liposomes are routinely stored at these temperatures for extended periods of time (Figure 6C).

After the stability of both liposomes would have been measured, the efficacy of the Erlotinib- and Gefitinib-encapsulated liposomes in combination with CNL would be measured to investigate if encapsulation exerts any influence on the effectiveness of the combination. The same exact protocol as before would be followed using the encapsulated EGFR inhibitors. UNC-7 and SCC-25 cells would be pre-treated with the same concentration range of either the Erlotinib liposomes or the Gefitinib liposomes for one hour, after which the same concentration range of CNL would be added. The resulting cell viability would be assessed at 24 and 48 hours post-CNL treatment. This study predicts that at both time points in both cell lines, encapsulation would have no effect on the efficacy of both drug combinations. It is anticipated that the results for both liposomes would appear near-identical to those depicted in Figure 2.

Production of Cetuximab-Conjugated CNL

In order to facilitate conjugation of Cetuximab to the surface of the CNL, the component 1,2-distearoyl-sn-glycero-3- phosphoethanolamine-N-[maleimide(polyethylene glycol)-2000] (DSPE-PEG(2000) Maleimide) was added to the CNL formulation. This lipid component is similar in structure to a standard DSPE-PEG(2000) as used in the Erlotinib and Gefitinib liposomes, but they contain an additional reactive maleimide group that can crosslink with thiol groups on the constant region of monoclonal antibodies. The lipid formulation and associated molar ratios were graciously provided by the Kester Lab, and under their guidance, the formulation was altered slightly to accommodate the addition of DSPE-PEG(2000) Maleimide to the liposomal backbone at a molar ratio comprising 1% of the total liposome composition. Figure 7 displays each of the components and their molar ratios for the CNL-maleimide liposome. Each of the components were combined and the thin-film hydration method followed by extrusion with a 100 nm Nuclepore^{TM} filter were used to form liposomes approximately 90-100 nm in size. Following extrusion, liposome size and zeta potential were measured by Dynamic Light Scattering (DLS). Size-exclusion column chromatography was used to separate the liposomes from the non-encapsulated drug in the surrounding solution before liposomal aliquots were given to Dr. Todd Fox in the Kester Lab for encapsulation efficiency measurement by mass spectrometry. Figure 7 shows the results for a successful batch of the CNL-maleimide liposomes.

CNL-Maleimide Liposome

Lipid	Molar Ratio
DSPC	3.71
DOPE	1.73
PEG-2000	0.74
PEG-Maleimide	0.1
PEG-750-C8	0.74
Ceramide	2.97

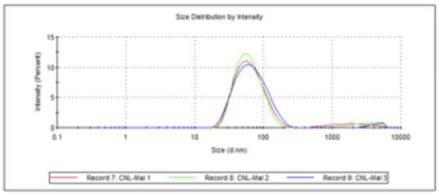

Size (nm)	ζ-Potential (mV)	Encapsulation Efficiency (%)
60.55	n.d.	24.6

Figure 7. Lipid composition, size, and encapsulation efficiency for CNLs modified to contain maleimide phospholipids. DLS was used to measure the size distribution of the CNL-maleimide liposomes. The left table displays the relative quantities of each lipid component in the formulation as a molar ratio. The center figure shows the size distribution by intensity of the produced batch of liposomes. Three measurements were collected during the sizing of the liposome batch. The right table displays the average size of the liposomes in the batch and its encapsulation efficiency. Encapsulation efficiency was measured using mass spectrometry. ζ-potential was not measured due to technical equipment difficulties.

The diameter of the CNL-maleimide liposomes was measured to be 60.1 nm ± 0.6 nm (Figure 7). This size is markedly smaller than the pore size of the 100 nm filter. The size distribution of the liposomes were measured to be appropriately bell-shaped and relatively narrow (Figure 7). Due to the combination of user error and virtual education constraints, zeta potential data were not available. The encapsulation efficiency was measured to be 24.6%, which nearly fits the target range of 25-30% (Figure 7). These results were communicated to the Kester Lab, during which it was brought to this study's attention that optimal conjugation can be achieved when it is attempted immediately after liposome extrusion. As such, this study planned to create a second batch of CNL-maleimide liposomes to attempt and optimize the maleimide conjugation protocol before progress was interrupted by the COVID-19 pandemic. Rather than attempt conjugation with Cetxuimab and potentially waste drug, conjugation would have first been attempted using a generic IgG antibody. Once the conjugation and validation protocols were optimized with the generic IgG, conjugation would have been attempted with Cetuximab.

Efficacy of Cetuximab-Conjugated CNL

This section was part of this study's original specific aims. However, due to the interruption by the transition to virtual education, it was not completed. The study's planned protocol and anticipated results will still be addressed.

Following successful conjugation of Cetuximab to the CNL surface, the efficacy of the Cetuximab-conjugated CNL would be measured to investigate if conjugation has any impact on cell viability relative to Cetuximab and CNL combined separately. A similar protocol as before would be followed using the Cetuximab-conjugated CNL. As Cetuximab is now conjugated to CNL, cells can no longer be pre-treated with Cetuximab for an hour prior to CNL addition. As such, UNC-7 and SCC-25 cells would be treated with a concentration range of Cetuximab-conjugated CNL, measuring the resulting cell viability at 24 and 48 hours post-treatment. This study predicts that at both time points in both cell lines, conjugation would have no effect on the efficacy of the combination of Cetuximab and CNL. It is anticipated that the results would appear near-identical to those depicted in Figure 2.

Discussion

In this study, HNSCC cell lines were treated with CNL and EGFR-inhibitors Erlotinib, Gefitinib, and Cetuximab to evaluate the efficacy of each individual agent. CNL was far more effective at decreasing HNSCC cell viability compared to the three EGFR inhibitors, suggesting that CNL has great potential as a monotherapy for HNSCC. To determine if CNL could sensitize HNSCC cells to each EGFR inhibitor, cells were treated with the combination of CNL and Erlotinib, Gefitinib, or Cetuximab. A synergistic effect was identified between CNL and Erlotinib and, more strongly, CNL and Gefitinib, while an additive effect was observed between CNL and Cetuximab. Synergy between CNL and either of the two EGFR inhibitors occurred most prominently at high concentrations of the EGFR inhibitors (10 or 25 uM) and middle concentrations of CNL (5 or 10 uM). The lack of efficacy of Cetuximab as either a monotherapy or in combination with CNL was an anticipated result for this study, as prior research has commented on Cetuximab's lack of efficacy in *in vitro* HNSCC models compared to *in vivo* models (Chang et al., 2015; Hartmann et al., 2016). The presence of a synergistic effect between CNL and both Erlotinib and Gefitinib suggests great therapeutic potential for these combinatorial treatments. These initial studies additionally establish CNL combined with Erlotinib or Gefitinib as a more efficacious treatment than Cetuximab alone in *in vitro* HNSCC models.

In light of the synergistic cell death effect discovered by this study, the molecular mechanism behind this effect remains to be elucidated. Ceramide, among other sphingolipids, has been shown to influence cell fate through modulation of several EGFR downstream signaling pathways that control cell growth and cell survival. Previous research has indicated that ceramide acts as a negative regulator in the AKT signaling cascade through direct AKT dephosphorylation, inhibiting cell cycle progression, promoting apoptotic responses, and enhancing autophagy (Wee and Wang, 2017). CNL specifically has also been shown to have an inhibitory effect on STAT3 signaling in cancer cell models. This reduction of

STAT3 phosphorylation reduces levels of critical anti-apoptotic proteins and induces cell death (Doshi et al., 2017). Conversely, treatment with EGFR inhibitors, specifically Gefitinib, was previously found to significantly increase phosphorylation of STAT3 in cancer cells, which increased the transcription and regulation of pro-survival pathways (Wen et al., 2015). This prior work provides a rationale behind both the lack of response to Gefitinib alone and the emergence of a synergistic effect after addition of CNL. STAT3 phosphorylation potentially serves as a compensatory resistance mechanism against treatment with Gefitinib, but subsequent addition of CNL inhibits STAT3 phosphorylation, leading to synergistic cell death. Future studies should further investigate how the STAT3/AKT pathways change in response to treatment with CNL + EGFR inhibitors to determine if they play a role in synergistic cell death.

In addition to elucidating the molecular mechanism behind the synergistic effect between CNL and Erlotinib/Gefitinib, further work is needed to explore why CNL failed to synergize with Cetuximab. One direction that could be pursued would be investigating how each of the EGFR inhibitors impact ceramide metabolism. Prior research in the field has found that various small molecule inhibitors can increase the expression and/or activity of ceramide synthase (CerS) family members, specifically CerS1, CerS5, and CerS6 (Jin et al., 2009; Schiffmann et al., 2010; Separovic et al., 2013). These specific CerS family members are responsible for synthesizing C_{16}- (CerS5, 6) and C_{18}- (CerS1) chain length ceramides (Mullen et al., 2012), which have been implicated in inducing cancer cell death (Henry et al., 2013), including in HNSCC (Senkal et al., 2006). Since Cetuximab and Erlotinib/Gefitinib selectively target different EGFR domains on different sides of the cell membrane, regulation of CerS family members could also differ between these two groups. Future studies should not only determine how Erlotinib, Gefitinib, and Cetuximab impact the expression and activation of CerS family members, but also investigate if the exogenous C_6-ceramide delivered by the CNL is metabolized into more pro-apoptotic chain length lipids, producing the synergistic cell death effect observed in this study.

Following the encouraging results above, this study sought to prepare both Erlotinib and Gefitinib for the transition into *in vivo* studies. Prior work in the field had established the physiological residence time for both EGFR inhibitors to be within the window of 24-48 hours, while evidence had been found that both drugs could also become phagocytosed or deactivated by the host's immune system after injection into the bloodstream (Lu et al., 2006; Ranson and Wardell, 2004). Considering how this study found that the synergistic effect between CNL with both EGFR inhibitors was strongest at the 48-hour time point, a solution was sought out to ensure optimal delivery of the therapeutic payload. Liposomal encapsulation is well-established as a method to both increase pharmacological bloodstream retention and shield from immune system detection (Bally et al., 1990; Gabizon and Papahadjopoulos, 1988; Klibanov et al., 1990). Therefore, this study shifted its focus to achieving successful and efficient encapsulation of Erlotinib and Gefitinib to enhance *in vivo* drug delivery. Multiple batches of Erlotinib- and Gefitinib-encapsulated liposomes were produced. The second batch appeared to be the most successful, with diameters close to the target value of 90 nm and a near optimal encapsulation efficiency for the Gefitinib liposome. The Erlotinib liposome struggled to encapsulate therapeutically relevant quantities of Erlotinib. One reason behind this shortcoming is believed to be that Erlotinib was not fully soluble in chloroform at the stock concentration used in this study. Dissolution in DMSO was deemed to be impossible for use in the thin-film rehydration method because of complications surrounding the time required to evaporate DMSO. Future studies should re-attempt Erlotinib encapsulation using a lower stock concentration in chloroform that promotes full Erlotinib dissolution and further investigate how to optimize the formulation of this liposome to maximize encapsulation efficiency. Progress was halted before the stability of both liposomes was measured as a function of BSA protein concentration, pH, and temperature. Future studies should look to adapt the methods established here to complete these measurements and begin to evaluate these combinatorial therapies *in vivo.*

Despite Cetuximb's lack of efficacy as a single agent and the absence of a synergistic effect between Cetuximab and CNL, Cetuximab still possesses utility independent of its therapeutic efficacy. Conjugation of Cetuximab to the surface of the CNL can serve as a HNSCC-specific targeting mechanism *in vivo*. As HNSCC tissue demonstrates increased EGFR expression and protein levels relative to healthy head and neck tissue, Cetuximab will bind in higher concentration to HNSCC tissue and inhibit EGFR

while delivering its conjugated CNL. In addition to this targeting effect, the structure of Cetuximab also has the potential of mobilizing the host immune system to assist in attacking the cancerous tissue (Mehra et al., 2008; Pozzi et al., 2016). As such, this study proceeded with the intent of creating a Cetuximab-conjugated CNL. The CNL formulation was successfully altered to incorporate DSPE-PEG(2000) maleimide phospholipids capable of crosslinking with a monoclonal antibody; however, progress on this study was halted before conjugation was attempted and optimized successfully. As mentioned previously, future studies should ensure that conjugation is attempted immediately after CNL-maleimide extrusion, as to ensure maximal CNL-antibody crosslinking. Future studies should additionally use the conjugation and validation methods outlined in this study to successfully produce a Cetuximab-conjugated CNL and evaluate the combinatorial therapy *in vivo*. Given the strong efficacy of CNL *in vitro* established by this study in addition to the variable efficacy of Cetuximab *in vivo* the development of a dual therapy between these two drugs in HNSCC has immense potential.

This study identified a novel effect between CNL and two EGFR inhibitors, Erlotinib and Gefitinib. This study also began the production of two separate drug delivery systems, encapsulating Erlotinib and Gefitinib inside liposomal delivery vehicles and taking steps toward creating a Cetuximab-conjugated CNL. While this study provides valuable information, it was cut short by the COVID-19 pandemic. As such, it is important that this research be continued in order to better understand and validate the conclusions that were made. Further research needs to occur to validate and optimize the liposome formulations used to encapsulate Erlotinib and Gefitinib. Furthermore, additional analysis and trials should be conducted to better understand the synergistic effect between CNL and Erlotinib/Gefitinib and how it can help combat HNSCC. Lastly, actual trials need to be conducted to test the success of the maleimide encapsulation method and the stability measurement method. Even with the unforeseen time limitation brought upon by COVID-19, this research has laid the groundwork for future studies to be able to develop a HNSCC targeted liposome.

Materials and Methods

Cell Culture and Materials

Two HNSCC cell lines were selected for this study: UNC-7 and SCC-25. UNC-7 was derived from oral cavity carcinomas and SCC-25 was derived from tongue carcinomas. Both cell lines are HPV negative and plated in DMEM/F12 media supplemented with 10% Fetal Bovine Serum (FBS). All cell lines were stored in an incubator at 37°C and 5% CO2. Proper sterile techniques were maintained throughout all cell culture procedures. Erlotinib, Gefitinib, and Cetuximab were procured from Selleck Chemicals. For cell viability experiments, Erlotinib and Gefitinib were resuspended in 100% dimethyl sulfoxide (DMSO) at stock concentrations of 9 mM and 20 mM, respectively. The control concentrations for Erlotinib and Gefitinib were delivered as a dilution of 100% DMSO equivalent to that of 25 μM of each drug. For use in the liposome formulations, Erlotinib and Gefitinib were resuspended in 100% chloroform at the same stock concentrations as before. Cetuximab was delivered pre-suspended in Phosphate Buffered Saline (PBS) at a stock concentration of 5.21 mg/mL. The control concentration for Cetuximab was delivered as pure PBS. All lipid components were obtained from Avanti Polar Lipids. CNL were obtained from the Kester Lab at the University of Virginia, produced using the materials and methods described by Stover and Kester (Stover and Kester, 2003). CNLs were stored at 4°C in 100% PBS at a stock concentration of 8.802 mM. The control for CNL was delivered as a ghost liposome containing the exact same liposome formulation minus C6-ceramide. Ghost liposomes were stored under the same conditions as CNL.

MTS Cell Viability Assays

Cells were seated at 5,000 cells per well into 96-well plates. Only the inner 60 wells were used, leaving the outer 36 empty, and two background wells of cell culture media were included in each plate. The cells were allowed to attach overnight. Concentrations of 0, 0.5, 1, 5, 10, and 25 μM (Erlotinib and Gefitinib) or 0, 10, 25, 50, 75, 100, 150, and 250 μg/mL(Cetuximab) were prepared from stock. Concentrations of 0,

2.5, 5, 10, and 25 μM were prepared for CNL from stock. The appropriate plates were treated with a concentration gradient of Erlotinib, Gefitinib, or Cetuximab. The plates were then incubated at 37°C for one hour to allow the inhibitors to reach their targets and the cells to become acclimated. Each plate was then treated with the CNL concentration gradient and placed back in the 37°C incubator. Two technical replicates were collected for each drug combination in a biological replicate. Twenty-four hours post-CNL treatment, MTS reagent was combined with PMS reagent in a ratio of 20 parts MTS to 1-part PMS. The MTS mixture is internalized by cells and serves as a substrate for NAD(P)H-dependent dehydrogenase enzymes, producing a brown formazan product. The amount of formazan produced positively correlates to cell viability. The MTS-PMS combination was then added to each well in the 24-hour plates, including the background wells. A Cytation3 plate reader was used to measure the absorbance of each plate at 490 nm. The plates were read each hour post MTS mixture addition until the double-negative control wells approached an absorbance of approximately 1.000. If the wells never reached 1.000, the absorbance values at the 3-hour mark were recorded and saved. This process was completed again for the other plates at 48-hours post-treatment. For a single plate to be analyzed, the absorbance of the background wells was first subtracted from each well's absorbance. Then each of the wells were normalized to the absorbance of the double-negative condition (0μM CNL, 0 Erlotinib/Gefitinib/Cetuximab). All of the technical replicates for the biological replicates were averaged together and displayed graphically.

Bliss Synergy Analysis

To statistically analyze the synergistic potential of each drug combination, a Bliss synergy score was calculated. This score compares the effect of each of the drugs alone to that of the combined effect to determine whether or not a combination is synergistic (score > 0), purely additive (score = 0), or antagonistic (score < 0). The SynergyFinder web application developed by Ianevski et al. (2017) was used to generate Bliss scores (Ianevski et al., 2017). Data was prepared for the web application as instructed by Ianevski et al.

Thin-Film Hydration Method, Liposome Extrusion, and Size-Exclusion Chromatography

The lipid components of appropriate ratios were combined in 10 mL glass tubes and placed in a heated nitrogen dryer until the lipids were completely dried. At minimum, drying persisted for two hours. Once dried, the lipids were rehydrated with 1 mL of PBS and the tube was placed in a shaking heat block at 60°C and 750 rpm to promote the spontaneous formation of liposomes. For a period of two hours on the shaking heat block, the tube was removed and vortexed for 10 seconds every 15 minutes to ensure that all lipids were stripped from the inner walls of the tube. During the shaking heat block incubation period, the liposome extrusion apparatus was cleaned and assembled. The extruder was warmed to 60°C. The syringes, teflon extrusion pieces, rubber O-rings, and metal locking mechanism were all thoroughly washed with distilled water and ethanol before being allowed to dry. Drying was facilitated by placing each piece on the now warm extruder. Once dry, the teflon extrusion pieces were placed inside the metal locking mechanism with a 0.1 μm Nuclepore filter placed in between, additionally sandwiched between two thin wafer filters. The locking mechanism was tightened to ensure minimal fluid leakage during extrusion and was snapped into place on the extruder to warm the locking mechanism to near 60°C. Additionally the syringes were inserted into the sides of the teflon pieces within the locking mechanism to ensure their warming to near 60°C as well. After ensuring that no lipid remained on the walls of the glass tube, liposomes were placed in a 60°C sonic water bath to be sonicated by hand for 10 minutes. The tube was moved around the water bath and placed in areas containing maximal sonic energy. Following sonication, the contents of one tube was loaded into the extraction apparatus while additional tubes were placed back in the shaking heat block. The liposome solution was passed through the filter a total of 13 times, after which the extruded liposomes were transferred to a 1.5 mL centrifuge tube, liposome size and zeta potential were measured, and the sample was stored at 4°C. Between the extrusion of each type of liposome, all components of the extruders were thoroughly washed with distilled water and ethanol and allowed to dry. To separate liposomes from the nonencapsulated drug in solution, a chromatography column was washed with distilled water and packed with size-exclusion beads. Once the column was packed to a specific height, the column was washed with PBS, after which, one liposome sample was

loaded into the column. The sample was allowed to fully enter the column, after which the column loading funnel was filled with PBS to facilitate sample movement through the column. The eluate was carefully watched. Once an opalesque eluate was observed, a 2 mL centrifuge tube was used to collect the eluate until the opalesque color disappeared. The resulting purified samples were stored at 4°C until small aliquots were prepared for encapsulation efficiency measurement.

Liposome Size and Encapsulation Efficiency Measurement

600 µL of PBS was added to 20 µL of a liposome sample in a plastic cuvette. The cuvette was placed inside a Malvern Zetasizer ZS90 and dynamic light scattering (DLS) was used to measure the size distribution of Erlotinib, Gefitinib, and CNL-maleimide liposomes. The Zetasizer collected three size measurements for each liposome sample. Following size measurement, zeta potential (surface charge) was also attempted to be measured. Throughout the majority of this study, zeta potential was measured using the same plastic cuvettes as those used for size measurement. However, shortly before COVID-19, the study was made aware that the plastic cuvettes did not deliver correct zeta potential results. It was planned to remeasure the zeta potential of all current liposome batches using cuvettes designed specifically for the measurement of zeta potential, but progress was derailed by COVID-19. To measure encapsulation efficiency, 100 µL aliquots of each liposome sample along with 250 µL aliquots of the corresponding nonencapsulated drugs dissolved in DMSO were prepared and handed off to Dr. Todd Fox in the Kester Lab. Dr. Fox used the nonencapsulated drugs to create a standard curve which was run through the mass spectrometer. Then the liposome sample corresponding to the nonencapsulated drug was run through the mass spectrometer and the standard curve was used to calculate the concentration of drug encapsulated inside the liposome. Dr. Fox reported the concentrations of each drug back to this study, which then used the volume of each liposome sample to calculate the µg of drug encapsulated inside the liposomes. To calculate encapsulation efficiency, µg encapsulated drug was divided by µg total drug added to the formulation and that value was multiplied by 100 to report encapsulation efficiency as a percent.

Liposome Stability Measurement

A total of nine 50 µL aliquots for each liposome would have been created to test the stability of the Erlotinib- and Gefitinib- encapsulated liposomes placed in different conditions. The conditions being tested would have been BSA protein concentration, pH level, and temperature. To measure stability as a function of BSA protein concentration, solutions of 0% (100% PBS), 14%, and 50% BSA would be created. One 50 µL aliquot from each liposome would be combined with 50 uL of each BSA solution inside a 600 µL microcentrifuge tube, bringing the protein concentration in the final solutions to 0%, 7%, and 25%. All aliquots would be stored at room temperature. A similar process would be used for pH stability testing, only this time the added solution would contain a different pH. The pH levels chosen for this study are 1 (stomach), 7.4 (blood), and 9 (gastrointestinal tract), which correspond to regions of the body these liposomes could potentially be exposed to. To achieve these pH levels, the solutions created would most likely have been 100 mM HCl, which has an approximate pH of 1, PBS, which has a pH of 7.4, and a solution of baking soda and deionized water, which could achieve a pH of 9. All aliquots would also be kept at room temperature. To measure how varying temperatures would have impacted liposome stability, one aliquot from each liposome would have been placed in a 4°C refrigerator, left at room temperature, and placed in a 37°C incubator. To maintain volume consistency with the other two stability measurements, each 50 µL aliquot used in temperature testing would be combined with 50 µL PBS. The size and zeta potential of the samples subjected to each of the conditions would be measured weekly by DLS to track changes in liposome stability over the course of one month.

Maleimide Conjugation

A generic IgG antibody and Cetuximab would have been conjugated to the surface of the CNL using methods described by Lu et al. (Lu et al., 2018). Cetuximab and maleimide CNLs would have been mixed at a molar ratio of 1:10 with continuous stirring for four hours. The thiol groups on Cetuximab would react with the maleimide groups on the CNL's surface, forming crosslinks. Successful conjugation of Cetuximab to the CNL would have been confirmed using the gel electrophoresis methods described by Loomis et al. (Loomis et al., 2010). Conjugates would have been run on a polyacrylamide gel, transferred

to a PVDF membrane, and stained for total protein. If successful conjugation was achieved, the total protein stain would have binded to the antibody-liposome conjugates and appear on the stain.

Figures and Statistics

All data was analyzed and figures were created using Microsoft Excel. The statistical software R was used to perform statistical analysis on the raw cell viability data. One-Way Analysis-of-Variance (ANOVA) tests and Tukey's Tests for post-hoc analysis were performed using R for the single-agent EGFR inhibitors: Erlotinib, Gefitinib, and CNL. Two-Way Analysis-of-Variance (ANOVA) tests and Tukey's Tests for post-hoc analysis were performed using R for analysis of the combination data between EGFR-inhibitors and CNL. Significant differences are visually noted using stars on the relevant bar graphs for the cell viability data. The following scheme is instituted for representing significance for the ANOVA and Tukey's tests: '***' indicates a p-value range of [0, 0.001), '**' p-value range of [0.001, 0.01), and '*' indicates a p-value range of [0.01, 0.05).

References

1. Adiseshaiah, P.P., Clogston, J.D., McLeland, C.B., Rodriguez, J., Potter, T.M., Neun, B.W., Skoczen, S.L., Shanmugavelandy, S.S., Kester, M., Stern, S.T., et al. (2013). Synergistic combination therapy with nanoliposomal C6-ceramide and vinblastine is associated with autophagy dysfunction in hepatocarcinoma and colorectal cancer models. Cancer Lett. *337*, 254–265.
2. Bally, M.B., Nayar, R., Masin, D., Hope, M.J., Cullis, P.R., and Mayer, L.D. (1990). Liposomes with entrapped doxorubicin exhibit extended blood residence times. Biochim. Biophys. Acta BBA - Biomembr. *1023*, 133–139.
3. Bray, F., Ferlay, J., Soerjomataram, I., Siegel, R.L., Torre, L.A., and Jemal, A. (2018). Global cancer statistics 2018: GLOBOCAN estimates of incidence and mortality worldwide for 36 cancers in 185 countries. CA. Cancer J. Clin. *68*, 394–424.
4. Byeon, H.K., Ku, M., and Yang, J. (2019). Beyond EGFR inhibition: multilateral combat strategies to stop the progression of head and neck cancer. Exp. Mol. Med. *51*, 1–14.
5. Chang, J.W., Kang, S.U., Shin, Y.S., Seo, S.J., Kim, Y.S., Yang, S.S., Lee, J.-S., Moon, E., Lee, K., and Kim, C.-H. (2015). Combination of NTP with cetuximab inhibited invasion/migration of cetuximab-resistant OSCC cells: Involvement of NF-κB signaling. Sci. Rep. *5*, 1–12.
6. Chen, L.F., Cohen, E.E.W., and Grandis, J.R. (2010). New Strategies in Head and Neck Cancer: epidermal growth factor receptor inhibition in head and neck cancer. Clin. Cancer Res. Off. J. Am. Assoc. Cancer Res. *16*, 2489–2495.
7. Dhule, S.S., Penfornis, P., He, J., Harris, M.R., Terry, T., John, V., and Pochampally, R. (2014). The Combined Effect of Encapsulating Curcumin and C6 Ceramide in Liposomal Nanoparticles against Osteosarcoma. Mol. Pharm. *11*, 417–427.
8. Doshi, U.A., Shaw, J., Fox, T.E., Claxton, D.F., Loughran, T.P., and Kester, M. (2017). STAT3 mediates C6-ceramide-induced cell death in chronic lymphocytic leukemia. Signal Transduct. Target. Ther. *2*, 1–12.
9. Gabizon, A., and Papahadjopoulos, D. (1988). Liposome formulations with prolonged circulation time in blood and enhanced uptake by tumors. Proc. Natl. Acad. Sci. *85*, 6949–6953.
10. Grandis, J.R., Melhem, M.F., Gooding, W.E., Day, R., Holst, V.A., Wagener, M.M., Drenning, S.D., and Tweardy, D.J. (1998). Levels of TGF-α and EGFR Protein in Head and Neck Squamous Cell Carcinoma and Patient Survival. JNCI J. Natl. Cancer Inst. *90*, 824–832.
11. Hartmann, S., Neckel, N., Seher, A., Mutzbauer, G., Brands, R.C., Linz, C., Kübler, A.C., and Müller-Richter, U.D.A. (2016). Erlotinib and gefitinib responsiveness in head and neck cancer cell lines—a comparing analysis with cetuximab. Clin. Oral Investig. *20*, 759–769.
12. Henry, B., Möller, C., Dimanche-Boitrel, M.-T., Gulbins, E., and Becker, K.A. (2013). Targeting the ceramide system in cancer. Cancer Lett. *332*, 286–294.
13. Ianevski, A., He, L., Aittokallio, T., and Tang, J. (2017). SynergyFinder: a web application for analyzing drug combination dose–response matrix data. Bioinformatics *33*, 2413–2415.
14. Jiang, Y., DiVittore, N.A., Kaiser, J.M., Shanmugavelandy, S.S., Fritz, J.L., Heakal, Y., Tagaram, H.R.S., Cheng, H., Cabot, M.C., Staveley-O'Carroll, K.F., et al. (2011). Combinatorial therapies improve the therapeutic efficacy of nanoliposomal ceramide for pancreatic cancer. Cancer Biol. Ther. *12*, 574–585.
15. Jin, J., Mullen, T.D., Hou, Q., Bielawski, J., Bielawska, A., Zhang, X., Obeid, L.M., Hannun, Y.A., and Hsu, Y.-T. (2009). AMPK inhibitor Compound C stimulates ceramide production and promotes Bax redistribution and apoptosis in MCF7 breast carcinoma cells. J. Lipid Res. *50*, 2389–2397.
16. Kirby, C., Clarke, J., and Gregoriadis, G. (1980). Effect of the cholesterol content of small unilamellar liposomes on their stability in vivo and in vitro. Biochem. J. *186*, 591–598.
17. Klibanov, A.L., Maruyama, K., Torchilin, V.P., and Huang, L. (1990). Amphipathic

polyethyleneglycols effectively prolong the circulation time of liposomes. FEBS Lett. *268*, 235–237.
18. Kolesnick, R.N., and Krönke, M. (1998). Regulation of Ceramide Production and Apoptosis. Annu. Rev. Physiol. *60*, 643–665.
19. Loomis, K., Smith, B., Feng, Y., Garg, H., Yavlovich, A., Campbell-Massa, R., Dimitrov, D.S., Blumenthal, R., Xiao, X., and Puri, A. (2010). Specific Targeting to B Cells by Lipid-Based Nanoparticles Conjugated with a Novel CD22- ScFv. Exp. Mol. Pathol. *88*, 238–249.
20. Lu, J.-F., Eppler, S.M., Wolf, J., Hamilton, M., Rakhit, A., Bruno, R., and Lum, B.L. (2006). Clinical pharmacokinetics of erlotinib in patients with solid tumors and exposure-safety relationship in patients with non–small cell lung cancer. Clin. Pharmacol. Ther. *80*, 136–145.
21. Lu, L., Ding, Y., Zhang, Y., Ho, R.J., Zhao, Y., Zhang, T., and Guo, C. (2018). Antibody-modified liposomes for tumor-targeting delivery of timosaponin AIII. Int. J. Nanomedicine *13*, 1927–1944.
22. Mao, L., Hong, W.K., and Papadimitrakopoulou, V.A. (2004). Focus on head and neck cancer. Cancer Cell *5*, 311–316.
23. Mehra, R., Cohen, R.B., and Burtness, B.A. (2008). The Role of Cetuximab for the Treatment of Squamous Cell Carcinoma of the Head and Neck. Clin. Adv. Hematol. Oncol. HO *6*, 742–750.
24. Merrill, A.H.J., Schmeiz, E.M., Dillehay, D.L., Spiegel, S., Shayaman, J.A., Schroeder, J.J., Riley, R.T., Voss, K.A., and Wang, E. (1997). Sphingolipids--the enigmatic lipid class: biochemistry, physiology, and pathophysiology.
25. Mullen, T.D., Hannun, Y.A., and Obeid, L.M. (2012). Ceramide synthases at the centre of sphingolipid metabolism and biology. Biochem. J. *441*, 789–802.
26. O'Neil, B.H., Allen, R., Spigel, D.R., Stinchcombe, T.E., Moore, D.T., Berlin, J.D., and Goldberg, R.M. (2007). High Incidence of Cetuximab-Related Infusion Reactions in Tennessee and North Carolina and the Association With Atopic History. J. Clin. Oncol. *25*, 3644–3648.
27. Perez, C.A., Song, H., Raez, L.E., Agulnik, M., Grushko, T.A., Dekker, A., Stenson, K., Blair, E.A., Olopade, O.I., Seiwert, T.Y., et al. (2012). Phase II study of gefitinib adaptive dose escalation to skin toxicity in recurrent or metastatic squamous cell carcinoma of the head and neck. Oral Oncol. *48*, 887–892.
28. Pozzi, C., Cuomo, A., Spadoni, I., Magni, E., Silvola, A., Conte, A., Sigismund, S., Ravenda, P.S., Bonaldi, T., Zampino, M.G., et al. (2016). The EGFR-specific antibody cetuximab combined with chemotherapy triggers immunogenic cell death. Nat. Med. *22*, 624–631.
29. Ranson, M., and Wardell, S. (2004). Gefitinib, a novel, orally administered agent for the treatment of cancer. J. Clin. Pharm. Ther. *29*, 95–103.
30. Schiffmann, S., Ziebell, S., Sandner, J., Birod, K., Deckmann, K., Hartmann, D., Rode, S., Schmidt, H., Angioni, C., Geisslinger, G., et al. (2010). Activation of ceramide synthase 6 by celecoxib leads to a selective induction of C16:0-ceramide. Biochem. Pharmacol. *80*, 1632–1640.
31. Senkal, C.E., Ponnusamy, S., Rossi, M.J., Sundararaj, K., Szulc, Z., Bielawski, J., Bielawska, A., Meyer, M., Cobanoglu, B., Koybasi, S., et al. (2006). Potent Antitumor Activity of a Novel Cationic Pyridinium-Ceramide Alone or in Combination with Gemcitabine against Human Head and Neck Squamous Cell Carcinomas in Vitro and in Vivo. J. Pharmacol. Exp. Ther. *317*, 1188–1199.
32. Separovic, D., Breen, P., Boppana, N.B., Van Buren, E., Joseph, N., Kraveka, J.M., Rahmaniyan, M., Li, L., Gudz, T.I., Bielawska, A., et al. (2013). Increased killing of SCCVII squamous cell carcinoma cells after the combination of Pc 4 photodynamic therapy and dasatinib is associated with enhanced caspase-3 activity and ceramide synthase 1 upregulation. Int. J. Oncol. *43*, 2064–2072.
33. Sheu, J.J.-C., Hua, C.-H., Wan, L., Lin, Y.-J., Lai, M.-T., Tseng, H.-C., Jinawath, N., Tsai, M.-H., Chang, N.-W., Lin, C.-F., et al. (2009). Functional Genomic Analysis Identified Epidermal Growth Factor Receptor Activation as the Most Common Genetic Event in Oral Squamous Cell Carcinoma. Cancer Res. *69*, 2568–2576.

34. Sim, F., Leidner, R., and Bell, R.B. (2019). Immunotherapy for Head and Neck Cancer. Oral Maxillofac. Surg. Clin. N. Am. *31*, 85–100.
35. Soulieres, D., Senzer, N.N., Vokes, E.E., Hidalgo, M., Agarwala, S.S., and Siu, L.L. (2004). Multicenter Phase II Study of Erlotinib, an Oral Epidermal Growth Factor Receptor Tyrosine Kinase Inhibitor, in Patients With Recurrent or Metastatic Squamous Cell Cancer of the Head and Neck. J. Clin. Oncol. *22*, 77–85.
36. Stover, T., and Kester, M. (2003). Liposomal Delivery Enhances Short-Chain Ceramide-Induced Apoptosis of Breast Cancer Cells. J. Pharmacol. Exp. Ther. *307*, 468–475.
37. Stover, T.C., Sharma, A., Robertson, G.P., and Kester, M. (2005). Systemic Delivery of Liposomal Short-Chain Ceramide Limits Solid Tumor Growth in Murine Models of Breast Adenocarcinoma. Clin. Cancer Res. *11*, 3465–3474.
38. Tran, M.A., Smith, C.D., Kester, M., and Robertson, G.P. (2008). Combining Nanoliposomal Ceramide with Sorafenib Synergistically Inhibits Melanoma and Breast Cancer Cell Survival to Decrease Tumor Development. Clin. Cancer Res. *14*, 3571–3581.
39. Vermorken, J.B., Trigo, J., Hitt, R., Koralewski, P., Diaz-Rubio, E., Rolland, F., Knecht, R., Amellal, N., Schueler, A., and Baselga, J. (2007). Open-Label, Uncontrolled, Multicenter Phase II Study to Evaluate the Efficacy and Toxicity of Cetuximab As a Single Agent in Patients With Recurrent and/or Metastatic Squamous Cell Carcinoma of the Head and Neck Who Failed to Respond to Platinum-Based Therapy. J. Clin. Oncol. *25*, 2171–2177.
40. Vermorken, J.B., Mesia, R., Rivera, F., Remenar, E., Kawecki, A., Rottey, S., Erfan, J., Zabolotnyy, D., Kienzer, H.-R., Cupissol, D., et al. (2008). Platinum-Based Chemotherapy plus Cetuximab in Head and Neck Cancer. N. Engl. J. Med. *359*, 1116–1127.
41. Watters, R.J., Kester, M., Tran, M.A., Loughran, T.P., and Liu, X. (2012). Chapter five - Development and Use of Ceramide Nanoliposomes in Cancer. In Methods in Enzymology, N. Düzgüneş, ed. (Academic Press), pp. 89–108.
42. Wee, P., and Wang, Z. (2017). Epidermal Growth Factor Receptor Cell Proliferation Signaling Pathways. Cancers *9*.
43. Wen, W., Wu, J., Liu, L., Tian, Y., Buettner, R., Hsieh, M.-Y., Horne, D., Dellinger, T.H., Han, E.S., Jove, R., et al. (2015). Synergistic anti-tumor effect of combined inhibition of EGFR and JAK/STAT3 pathways in human ovarian cancer. Mol. Cancer *14*, 100.